Journal of Fluorine Chemistry 140 (2012) 70–75

Contents lists available at SciVerse ScienceDirect

Journal of Fluorine Chemistry

journal homepage: www.elsevier.com/locate/fluor

Synthesis and upconversion luminescence properties study of $NaYbF_4:Tm^{3+}$ crystals with different dopant concentration

Tao Jiang, Weiye Song, Shusen Liu, Weiping Qin *

State Key Laboratory on Integrated Optoelectronics, College of Electronic Science & Engineering, Jilin University, Changchun 130012, PR China

ARTICLE INFO

Article history:
Received 15 February 2012
Received in revised form 19 April 2012
Accepted 7 May 2012
Available online 11 May 2012

Keywords:
Ultraviolet
Upconversion luminescence
Na^+ cation
$NaYbF_4$

ABSTRACT

Tm^{3+} ion doped α-$NaYbF_4$ nanocrystals (NCs) and β-$NaYbF_4$ microcrystals (MCs) were prepared by one-step hydrothermal method through tuning pH values. Through the comparative study on the crystal growth mechanism guided by two different organic additives, the effect of Na^+ cation on morphologies was discussed. Under 980-nm excitation, intense ultraviolet (UV) and blue upconversion (UC) emissions were observed from both of them. The UC luminescence properties of the as-prepared MCs were studied based on changing the Tm^{3+} ion concentrations. The fluorescent lifetimes of MCs doped with different amount of Tm^{3+} ions indicate that the obtained $NaYbF_4:Tm^{3+}$ MC was an excellent matrix for UV UC emissions.

1. Introduction

With the advent of cheap laser diodes, the frequency upconversion (UC) of infrared (IR) radiation by suitable trivalent lanthanide ions (Ln^{3+}) combinations is of current interest [1–7]. UC is an anti-Stokes process in which low energy radiation, usually near infrared (NIR) or IR light, is converted to higher energy radiation such as ultraviolet (UV) or visible light via multiphoton absorptions or energy transfers (ETs). Insufficient intensities, however, constitute still the main limitation for practical applications of UC materials; especially efficient UV emissions via UC remain challenging because they require more than three participated NIR photons. It is well known that the luminescence properties of materials are significantly concerned with their morphologies, dimensionalities, and sizes. The rational control of morphology can be a feasible and efficient strategy in tuning their physical and chemical properties. Consequentially, plenty of inorganic materials with various morphologies have been synthesized with the purpose of seeking for high effective UC luminescence materials [8–11]. Morphology control has been performed by adjusting Ln^{3+}/F^- ratio, temperature, solvents, and organic additives [12–14], however, rare attention has been paid to the effect of cations on morphology. As an organic additive, trisodium citrate (TC) introduces more Na^+ ions into the reaction system and causes different morphologies, compared with citric acid (CA).

As conventional luminescence matrixes, the fluorides based on $NaREF_4$ (RE = rare earth ions) are currently under vigorous investigation due to their superior spectroscopic properties and potential applications in wide ranges of flat-panel display devices, short wavelength solid-state lasers, optical data storage, fluorescence imaging, drug deliver, and so on [15–19]. While $NaYF_4$ NCs or MCs have been generally demonstrated as the most promising UC luminescence materials, it is still imperative to explore other $NaREF_4$ crystals with high quality and fewer quenching centers to achieve high efficient UV UC emissions [20–24]. The excited state of Yb^{3+} ions locates at approximately 10,000 cm^{-1} and is resonant with 980 nm laser. When codoped with the other Ln^{3+} ions, Yb^{3+}, as an ideal sensitizer, can actively transfer the absorbed energy to the other codopants [25,26]. The doping concentration of Ln^{3+} ions is very important for getting efficient UV UC emissions. Much research on concentration tuning has been done using $NaYF_4$ and YF_3 matrixes [27,28], however the best doping concentration of Tm^{3+} in $NaYbF_4$ matrix has not been investigated in detail.

MCs and NCs have been synthesized through various methods such as high temperature thermal decomposition [29], microemulsion [30], high pressure [31], and hydrothermal/solvothermal [32,33] approaches. Compared with the other methods, hydrothermal treatment works at low reaction temperature with relatively simple equipments and processes. It also has advantages in preparing various inorganic materials with less pollution, high homogeneity, high purity, and controllable morphology.

In our study, Tm^{3+} ions doped α-$NaYbF_4$ nanospheres and β-$NaYbF_4$ microprisms (MPs) were prepared at different pH values by one-step hydrothermal method with TC or CA as the organic additives. The effect of Na^+ cation on morphologies was

* Corresponding author. Tel.: +86 431 8516 8241 8325; fax: +86 431 8516 8241 8325.
E-mail address: wpqin@jlu.edu.cn (W. Qin).

0022-1139/$ – see front matter © 2012 Elsevier B.V. All rights reserved.
http://dx.doi.org/10.1016/j.jfluchem.2012.05.005

investigated by comparing the reaction processes modified by the two different organic additives. Moreover, intense UV UC emissions were observed in both the NCs and the MPs, the visible and IR UC emissions from 500 nm to 900 nm were nearly vanished. The blue UC light from the MPs was easily visible to the naked eye in the daylight. The best doping concentration of Tm^{3+} ions in the MPs was confirmed as 1.5 mol%. The UC luminescence properties of the MPs were investigated by temporal evolution curves of UV and visible UC emissions.

2. Results and discussion

2.1. Phase identification and morphologies

Fig. 1(a) shows the typical XRD patterns of the as-prepared products synthesized at different pH values using TC as the organic additive. The product obtained at pH 3 is α-$NaYbF_4$, which is consistent with the literature value (JCPDS 77-2043). When the pH value increased to 7 or 10, the crystal structure changed to hexagonal phase $NaYbF_4$ (JCPDS 27-1427).

The representative FESEM images of these samples are shown in Fig. 1(b)–(d). The samples synthesized at pH 3 are nanospheres composed of a great deal of smaller particles with the diameters of 200–400 nm, as described in Fig. 1(b). It is noteworthy that large amount of emarginated MPs appeared as the pH value was adjusted to 7 (Fig. 1(c)). The average length and diameter of MPs are 8 μm and 2 μm. When the pH value increased to 10, the MPs were 4 μm in length and 3 μm in diameter. The concavity of their ends became more obvious.

The XRD patterns of products prepared by using CA at different pH values are shown in Fig. 2(a). The product obtained at pH 3 is β-$NaYbF_4$ (JCPDS 27-1427) mixed with α-$NaYbF_4$ (JCPDS 77-2043). All the diffraction peaks of products prepared at pH 7 and 10 can be indexed to pure β-$NaYbF_4$.

Fig. 2(b)–(d) represent the typical FESEM images of these samples. The samples synthesized in an acidic environment are long MPs mixed with NCs. The average length and diameter of the long MPs are 15 μm and 5 μm, respectively (Fig. 2(b)). High quality MPs were obtained as the pH value increased to 7, it can be seen clearly that there is a hexagonal groove on the top of the MPs and the average length and diameter of the MPs are 3 μm and 2 μm (Fig. 2(c)). When the pH value increased to 10, the MPs grow bigger with 4 μm in length and 3 μm in diameter and the morphologies of the MPs did not vary too much compared with that of the ones prepared at pH 7.

2.2. Growth mechanism

In a typical hydrothermal process using TC or CA as the chelating agent, first, the $H_{3-n}Cit^{n-}$ ions are combined with the added Ln^{3+} cations and form steady metal complexes owing to the strong chelation between them in the precursor solution. This can be confirmed by our experiment that a milky suspension have been observed in the aqueous solutions containing both Ln^{3+} cations and $H_{3-n}Cit^{n-}$ ions. When $NaBF_4$ is added into the reaction system under hydrothermal condition, the chelation of the RE^{3+}–citrate complex is weakened and RE^{3+} ions are released to form small primary crystal nuclei with $NaBF_4$ through the increase of the reaction temperature and the prolongation of reaction time under high pressure [34,35]. If the pH value of the liquid solution is changed, the existent form of the $H_{3-n}Cit^{n-}$ and the chelation between $H_{3-n}Cit^{n-}$ and the metal ions are affected. As a consequence, the morphologies of the obtained samples are tuned under different pH conditions [36,37]. However, morphologies are a little different between the samples using trisodium citrate or citric acid with different ionization degree under the same pH condition. When the environment is alkaline, $H_{3-n}Cit^{n-}$ exists as Cit^{3-} and so the chelation reaction between Ln^{3+} and Cit^{3-} is strengthened. However, if the pH decreases, the existent form of

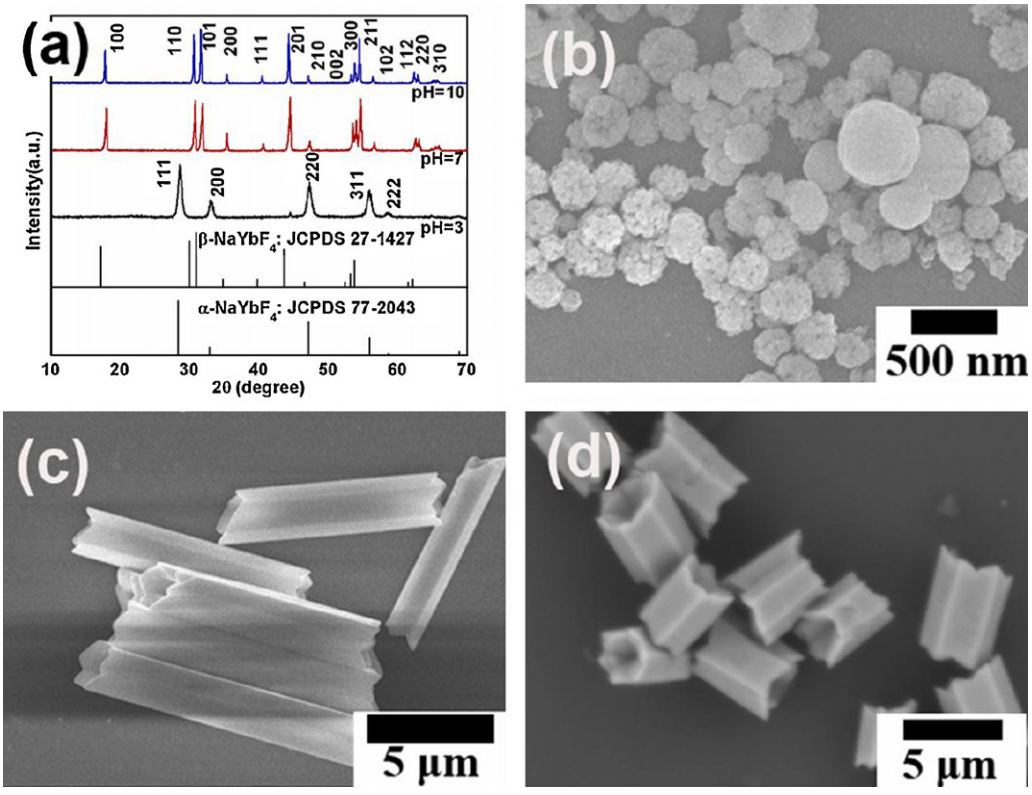

Fig. 1. (a) XRD patterns and (b–d) FE-SEM images of products modified by trisodium citrate at different pH values. The pH is 3 (b), 7 (c), and 10 (d), respectively.

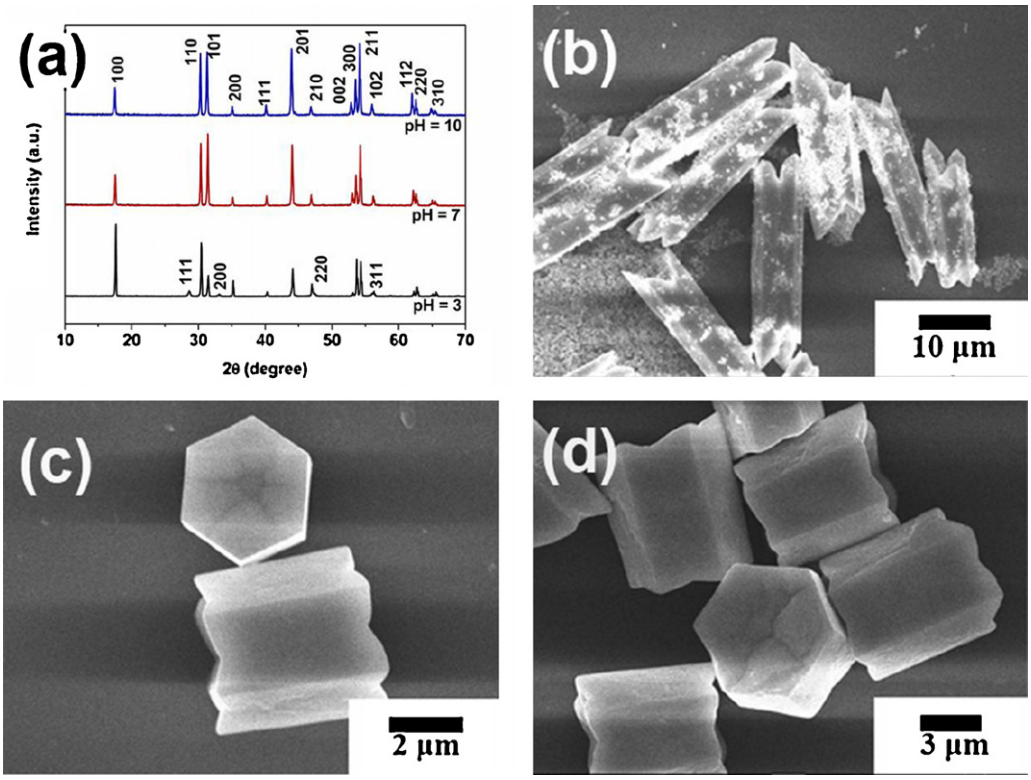

Fig. 2. (a) XRD patterns and (b–d) FE-SEM images of products modified by citric acid at different pH values. The pH is 3 (b), 7 (c), and 10 (d), respectively.

Cit^{3-} will change to $HCit^{2-}$, H_2Cit^-, or H_3Cit, and its chelation ability decreases significantly. As we have known that planes appear when the crystal faces possess the lowest growth rate compared with other faces. At different pH values, the surfaces of crystal occupied by Cit^{3-} are different, the surface energy is effectively reduced and the growth rate of different surfaces of crystals will differ from each other, then the anisotropic growth is induced dramatically, so the morphologies and the sizes of ultimate products are controlled. According to previous reports, citrate ions can adsorb on the facets of β-$NaYbF_4$ and prohibit the typical growth in the [0 0 0 1] direction [14]. Therefore $NaYbF_4$ evolved into well-defined crystallographic MPs with smooth surfaces.

Attention was paid to the condition that redundant Na^+ cations were introduced to the hydrothermal reaction when TC was used as the organic additive compared with CA. The Na^+ cations also have some effect on morphologies that they would selectively adsorb on the particular crystal facets of the growing crystals and change the growth rate of the crystalline plane. The effects of Na^+ cations can be confirmed by comparing the samples modified by the two different organic additives under the same acid condition (pH 3). The effect of different pH values is further discussed as follow:

2.2.1. TC

Under acid condition, Cit^{3-} existed as H_2Cit^- or H_3Cit and there was rare Cit^{3-} absorbed on the crystal surface, so the restraint effect on the {0 0 0 1} facets of $NaYbF_4$ crystal was weak. When the $NaBF_4$ was added, it hydrolyzed to $BO_3{}^{3-}$ and F^- anions as illustrated by the following reaction:

$$NaBF_4 + H_2O \rightarrow Na^+ + F^- + 3HF + H_3BO_3 \quad (1)$$

The excessive Na^+ cations introduced into the hydrothermal process by TC promoted the isotropic growth of the α-$NaYbF_4$ nuclei and suppressed the above reaction. As a result, the α-$NaYbF_4$ nuclei just grew to a spherical shape and did not increase along a special crystal axis determined by the absorbed organic group to transform to β-$NaYbF_4$ crystals.

Under neutral condition, Cit^{3-} existed as $HCit^{2-}$ or H_2Cit^-, the effect of Cit^{3-} became important and the phase of $NaYbF_4$ crystals changed from cubic to hexagonal, this process was considered as a disorder-to-order change, and then, the hexagonal crystals grew up simultaneously. Under alkaline condition, TC existed as Cit^{3-}. The inhibiting effect was obvious and the crystal growth along the (0 0 0 1) axial was slower, as a result, the β-phase MPs became flat gradually.

2.2.2. CA

Under acid condition, when $NaBF_4$ was added, the crystal growth along the {0 0 0 1} was accelerated by a small amount of absorbed Cit^{3+} ions and the reaction (1) processed effectively without excessive Na^+ cations, so most of the α-$NaYbF_4$ nuclei transformed to β-$NaYbF_4$ crystals with a large scale along the {0 0 0 1} crystal axis.

Under neutral or alkaline conditions, CA existed as $HCit^{2-}$ or Cit^{3-}, and the formation process of the MPs was the same with that of the ones produced by TC.

The pH of the precursor aqueous solution has been increased through adding $NH_3{\cdot}H_2O$ although it is also a chelating reagent [34,36]. The effect of $NH_3{\cdot}H_2O$ on the morphologies is not so important compared with that of the $H_{3-n}Cit^n$ existent form in this system. Further more, when NaOH aqueous solution was used, no product can be obtained properly due to the formation of another complex $Yb(OH)_x{}^{3-x}$, as a result, $NH_3{\cdot}H_2O$ was chosen.

2.3. UC luminescence properties

The UC luminescence spectra of different $NaYbF_4$:0.5 mol% Tm^{3+} samples are shown in Fig. 3 (modified by TC) and Fig. 4

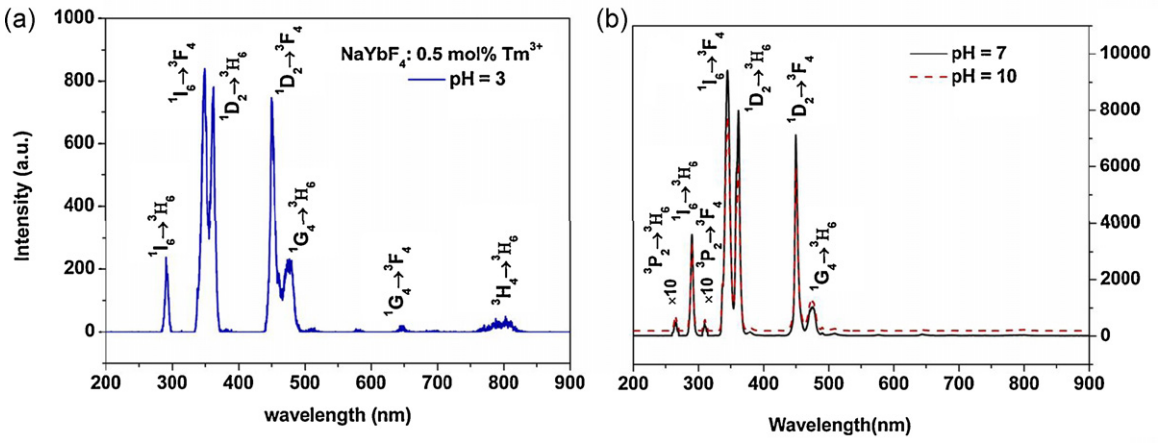

Fig. 3. UC luminescence spectra of crystals produced by trisodium citrate at different pH values under 980-nm excitation.

(modified by CA). Unusually, intense UV and weak visible UC emissions were observed both in the $NaYbF_4$ MPs and NCs. These UV UC emissions were observed to be centered at 264 nm, 291 nm, 309 nm, 347 nm, and 362 nm, which were attributed to the $^3P_2 \rightarrow {}^3H_6$, $^1I_6 \rightarrow {}^3H_6$, $^3P_2 \rightarrow {}^3F_4$, $^1I_6 \rightarrow {}^3F_4$, and $^1D_2 \rightarrow {}^3H_6$ transitions, respectively. Blue and green emissions were detected from the $^1D_2 \rightarrow {}^3F_4$, $^1G_4 \rightarrow {}^3H_6$, and $^1D_2 \rightarrow {}^3H_5$ transitions centered at approximately 450 nm, 476 nm, and 510 nm, respectively. The red and NIR UC emissions were observed to be centered at 576 nm, 643 nm, 689 nm, and 807 nm, which were from the $^1D_2 \rightarrow {}^3H_4$, $^1G_4 \rightarrow {}^3F_4$, $^3F_3 \rightarrow {}^3H_6$, and $^3H_4 \rightarrow {}^3H_6$ transitions, respectively. They were all the characteristic emission lines of Tm^{3+} ions excited by the ETs from Yb^{3+} ions. It can be seen that the 5-photon UC emission of $^1I_6 \rightarrow {}^3F_4$ was even stronger than the 4-photon UC emission of $^1D_2 \rightarrow {}^3F_4$ in Fig. 3. The $^1G_4 \rightarrow {}^3H_6$ and $^3H_4 \rightarrow {}^3H_6$ emissions almost vanished in Fig. 3(b). The ratios of UV/blue emissions in the TC modified MPs (TMPs) were larger than those modified by CA. First, it was probably due to the different local environment around the Ln^{3+} in the two different materials. Second, there were fewer luminescence quenching centers on the surfaces of TMPs, because TC had better ability in morphology control. All these conditions were better for the formation of stronger UV UC emissions.

Fig. 5 shows the detail population and photoluminescence processes in $NaYbF_4$:Tm^{3+} crystals. The pump light excites only the Yb^{3+} ions, the $^3H_5$, $^3F_2$, and $^1G_4$ levels are populated by three ETs from Yb^{3+} to Tm^{3+} with the increase of Tm^{3+} ions. The populated $^3F_2$ may nonradiatively relax to $^3F_3$ and $^3H_4$ levels, which produce 699 nm and 807 nm emissions. The $^1G_4$ level radiatively depopulate to $^3H_6$ and $^3F_4$ levels, which cause 476 nm and 643 nm emissions. And then, the $^1D_2$ level of Tm^{3+} is efficiently populated by the cross-relaxation (CR) process of $^3F_2 + {}^3H_4 \rightarrow {}^3H_6 + {}^1D_2$ between Tm^{3+} ions [38]. Subsequently, the electrons of $^1D_2$ level radiatively transfer to the ground-state and inter-states, which cause 362 nm, 450 nm, 510 nm, and 576 nm emissions. On the other hand, the electrons of the $^1D_2$ level may be excited to the $^3P_2$ level via another ET process, produce 265 nm and 309 nm emissions. The electrons of $^3P_2$ level usually transfer to $^1I_6$ level and emit 291 and 347 nm UV UC fluorescence efficiently. Radiative transitions from the $^3P_2$ level are difficult to occur owing to the rapidly nonradiative relaxation of the nearby $^3P_{0,1}$ and $^1I_6$ levels.

In order to find the appropriate Tm^{3+} concentration for the strongest UV UC emission intensities, the dependence of UC emissions on the Tm^{3+} concentrations was studied. Fig. 6(a) displays the UC emission spectra of $NaYbF_4$:*x*mol% Tm^{3+} TMPs at pH 7. The doped concentrations of Tm^{3+} ions are 0.3, 0.5, 0.8, 1.0, 1.5, 2.0, and 2.5 mol%, respectively. As can be seen from this figure that when the Tm^{3+} concentration is 1.5 mol%, UC emission intensities are the highest, and then they decrease sharply with increasing Tm^{3+} concentrations further due to concentration quenching. It is clearer that 291 nm, 347 nm, 362 nm, 450 nm, and 576 nm emissions get stronger with increasing Tm^{3+} concentrations from 0.3 to 1.5 mol% and then decrease as shown in Fig. 6(b). However, the intensities of 476 nm and 643 nm are the

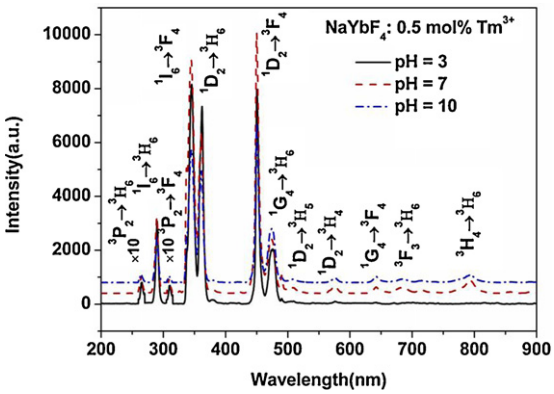

Fig. 4. UC luminescence spectra of crystals produced by citric acid at different pH values under 980-nm excitation.

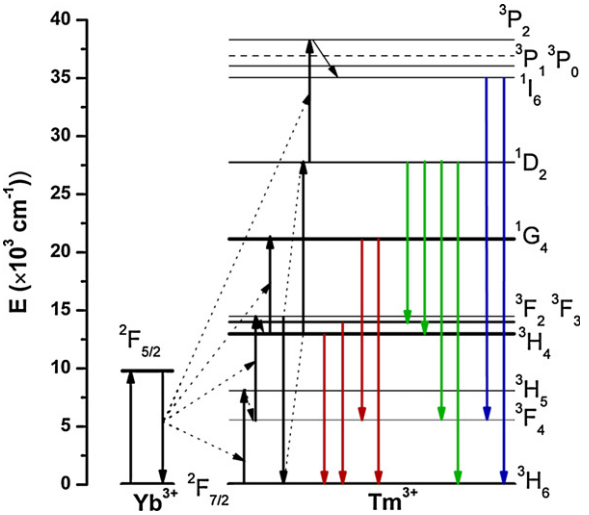

Fig. 5. UC mechanism of Yb^{3+}-sensitized Tm^{3+} emissions in the as-prepared samples.

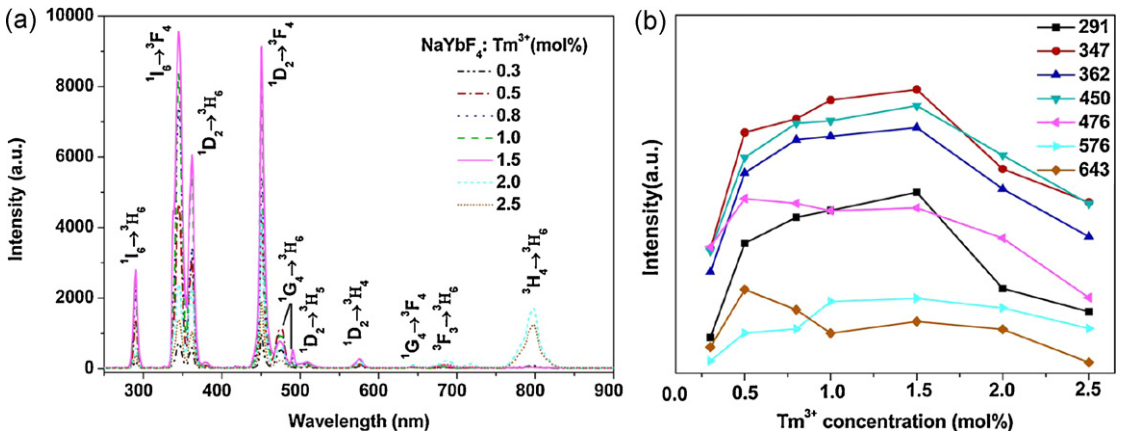

Fig. 6. (a) UC luminescence spectra and (b) variation of the UV and visible UC emissions depend on Tm^{3+} concentration of $NaYbF_4$:*x*mol% Tm^{3+} TMPs under neutral condition (*x* = 0.3, 0.5, 0.8, 1.0, 1.5, 2.0, and 2.5).

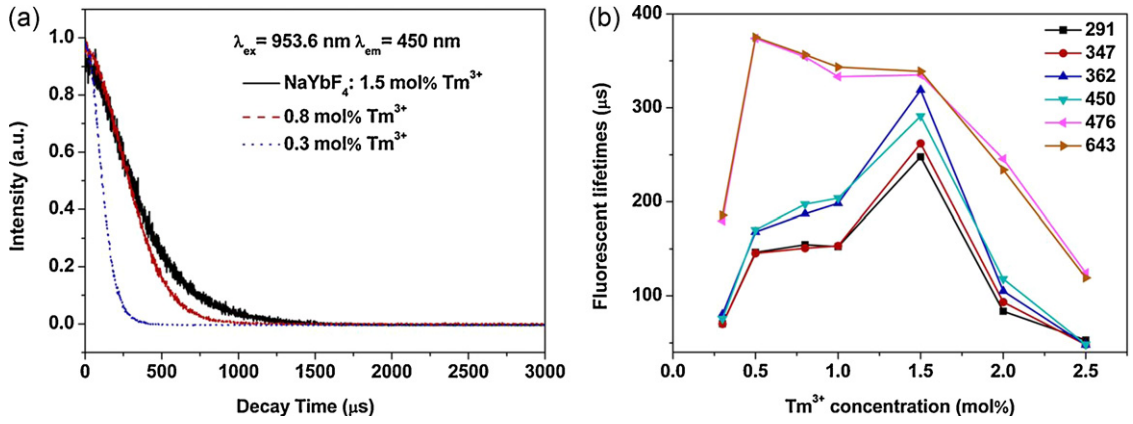

Fig. 7. (a) Luminescence decay curves of Tm^{3+} (λ_{ex} = 953.6 nm, λ_{em} = 450 nm, which represent the $^1D_2 \rightarrow {}^3F_4$ transition) and (b) variation of the UV and visible UC emission lifetimes in TMPs doped with different concentration of Tm^{3+} ions.

strongest at 0.5 mol% and then decrease gradually. This phenomenon can be explained as followed. In our group, we considered that the $^1D_2$ level were populated by the CR process of $^3F_2 + {}^3H_4 \rightarrow {}^3H_6 + {}^1D_2$ between Tm^{3+} ions, when the concentrations of Tm^{3+} ions increased, the CR process enhanced and so the amount of electrons reached $^1I_6$ and $^1D_2$ levels became large. The emission intensities of 4- and 5-photon process increased, gradually. At the same time, more electrons which reached $^1I_6$ and $^1D_2$ levels from $^3H_4$ level made the population of $^1G_4$ decrease and the radiative transition from $^1G_4$ level to $^3H_6$ level become inefficient. The emission intensity of 3-photon decreased as a result [27].

To further verify the mechanism related to the UC emission processes, luminescence decay curves of Tm^{3+} ions in TMPs were detected under a 953.6 nm pulsed Raman laser, respectively. For conciseness, only temporal evolutions of $^1D_2$ levels of Tm^{3+} ions in samples with doping concentrations as 0.3, 0.8, and 1.5 mol% are given in Fig. 7(a). These decay curves can be fitted well into exponential functions. All the lifetimes of Tm^{3+} ions in $NaYbF_4$ crystals with different doping concentrations are given in Table 1. The variation of fluorescent lifetimes of Tm^{3+} ions depend on the Tm^{3+} concentrations is shown in Fig. 7(b). It can be seen that the largest lifetimes of $^1I_6$ and $^1D_2$ levels were obtained when doped concentration of Tm^{3+} ions was 1.5 mol%, however, the largest lifetime of $^1G_4$ level appeared when 0.5 mol% was doped. The variation of fluorescent lifetimes consisted with the phenomenon that the intensities of the UC emissions were the highest when the doped Tm^{3+} concentration was 1.5 mol%.

Table 1
Deduced dynamic curve decay time constants of $NaYbF_4$ crystals doped with different concentration of Tm^{3+} ions.

λ_{em} (nm)	291	347	362	450	476	643
$\tau_{0.3\%\ Tm}$ (μs)	70	70	80	76	180	186
$\tau_{0.5\%\ Tm}$ (μs)	146	145	168	170	374	375
$\tau_{0.8\%\ Tm}$ (μs)	155	151	187	197	354	356
$\tau_{1.0\%\ Tm}$ (μs)	152	153	198	204	333	343
$\tau_{1.5\%\ Tm}$ (μs)	248	262	319	291	335	339
$\tau_{2.0\%\ Tm}$ (μs)	84	93	105	118	245	234
$\tau_{2.5\%\ Tm}$ (μs)	53	48	48	48	124	119

3. Conclusions

In summary, uniform, single-crystal nano- and micro-sized $NaYbF_4$:Tm^{3+} crystals were successfully synthesized via a simple hydrothermal method modified by CA or TC at different pH values. Intense UV UC emissions were observed in both the NCs and MPs. The best doping concentration of Tm^{3+} in the $NaYbF_4$ MPs for the highest UC emission intensity was confirmed as 1.5 mol%. The fluorescent lifetimes in the MPs with different concentrations of Tm^{3+} were also detected.

4. Experimental details

All the rare earth nitrates used for the synthesis were of 99.999% purity. The other chemicals were of analytical grade reagents and used directly without further purification.

4.1. Sample preparation

In a typical synthesis, 1 mmol of $Ln(NO_3)_3$ (Ln = Yb, Tm) was mixed with 10 ml of TC or CA (0.1 M) aqueous solution under vigorous stirring for 1 h. 10 ml $NaBF_4$ (1.25 M) aqueous solution was then added slowly into the above solution. After stirred for another 20 min, the as-obtained precursor solution was transferred to a 40 ml autoclave, sealed and maintained at 180 °C for 24 h. After reacting, the system was allowed to cool to room temperature naturally. The resulting precipitates were separated by centrifugation, washed with deionized water and ethanol by several times, and then dried in air at 80 °C for 12 h. $NaYbF_4$ nanospheres and $NaYbF_4$ MPs were synthesized by the same method through using different organic additives at various pH values. The pH of the precursor aqueous solution was adjusted by adding $NH_3 \cdot H_2O$ or HNO_3 solution.

4.2. Characterization

The purity and phase structure of the products were identified by X-ray diffraction (XRD) using a Model Rigaku Ru-200b powder diffractometer with nickel-filtered Cu-Kα radiation (λ = 1.5406 Å). The operation voltage and current were 50 kV and 200 mA, respectively. The 2θ angle ranges from 10° to 70°. The size and morphology of the products were observed by a JEOL JSM-6330F field emission scanning electron microscope (FESEM). The UC emission properties of the samples were examined by Hitachi F-4500 fluorescence spectrophotometer (1.0 nm for spectral resolution and 400 V for PMT voltage) using a 980 nm continuous laser diode (the power density is 320 W/cm^2) as the excitation source. The UC emission spectra were measured under the identical conditions in order to compare their relative emission intensities. All the analysis was performed at room temperature.

Acknowledgments

This work was supported by the National High Technology Research and Development Program of China (863 Program: 2009AA03Z309), the National Natural Science Foundation of China (NSFC) (grants 51072065, 0874058, 60908031, 60908001, 61077033) and the Program for New Century Excellent Talents in University (No: NCET-08-0243).

References

[1] F. Auzel, Chemical Reviews 104 (2003) 139–174.
[2] M. Haase, H. Schäfer, Angewandte Chemie International Edition 50 (2011) 5808–5829.
[3] F. Wang, Y. Han, C. Lim, Y. Lu, J. Wang, J. Xu, H. Chen, C. Zhang, M. Hong, X. Liu, Nature 463 (2010) 1061–1065.
[4] B. Gai, P. Yang, C. Li, W. Wang, Y. Dai, N. Niu, J. Lin, Advanced Functional Materials 20 (2010) 1166–1172.
[5] F. Wang, R. Deng, J. Wang, Q. Wang, Y. Han, H. Zhu, X. Chen, X. Liu, Nature Materials 10 (2011) 968–973.
[6] R. Deng, X. Xie, M. Vendrell, Y. Chang, X. Liu, Journal of the American Chemical Society 133 (2011) 20168–20171.
[7] F. Chen, W. Bu, S. Zhang, X. Liu, J. Liu, H. Xing, Q. Xiao, L. Zhou, W. Peng, L. Wang, J. Shi, Advanced Functional Materials 21 (2011) 4285–4294.
[8] S. Heer, K. Kömpe, H. Güdel, M. Haase, Advanced Materials 16 (2004) 2102–2105.
[9] H. Qian, Y. Zhang, Langmuir 24 (2008) 12123–12125.
[10] Y. Su, L. Li, G. Li, Crystal Growth and Design 8 (2008) 2678–2683.
[11] C. Li, J. Lin, Journal of Materials Chemistry 20 (2010) 6831–6847.
[12] D. Ma, S. Huang, Y. Yu, Y. Xu, Y. Dong, Journal of Physical Chemistry C 113 (2009) 8136–8142.
[13] C. Li, J. Yang, Z. Quan, P. Yang, D. Kong, J. Lin, Chemistry of Materials 19 (2007) 4933–4942.
[14] J. Zhao, Y. Sun, X. Kong, L. Tian, Y. Wang, L. Tu, J. Zhao, H. Zhang, Journal of Physical Chemistry B 112 (2008) 15666–15672.
[15] A. Stevenson, H. Serier-Brault, P. Gredin, M. Mortier, Journal of Fluorine Chemistry 132 (2011) 1165–1173.
[16] K. Zheng, D. Zhang, D. Zhao, N. Liu, F. Shi, W. Qin, Physical Chemistry Chemical Physics 12 (2010) 7620–7625.
[17] J. Chen, C. Guo, M. Wang, L. Huang, L. Wang, C. Mi, J. Li, X. Fang, C. Mao, S. Xu, Journal of Materials Chemistry 21 (2011) 2632–2638.
[18] Q. Ju, D. Tu, Y. Liu, R. Li, H. Zhu, J. Chen, Z. Chen, M. Huang, X. Chen, Journal of the American Chemical Society 134 (2012) 1323–1330.
[19] X. Xue, F. Wang, X. Liu, Journal of Materials Chemistry 21 (2011) 13107–13127.
[20] W. Niu, S. Wu, S. Zhang, Journal of Materials Chemistry 20 (2010) 9113–9117.
[21] Z. Wang, C. Liu, Y. Wang, Z. Li, Journal of Alloys and Compounds 509 (2011) 1964–1968.
[22] C. Cao, W. Qin, J. Zhang, Optics Communication 283 (2011) 547–550.
[23] Z. Wang, J. Hao, H. Chan, Journal of Materials Chemistry 20 (2010) 3178–3185.
[24] G. Chen, T. Ohulchanskyy, W. Law, H. Agren, P. Prasad, Nanoscale 3 (2011) 2003–2008.
[25] A. Oliveira, M. Araujo, A. Gouveia-Neto, J. Neto, A. Sombra, Y. Messaddeq, Applied Physics Letters 72 (1998) 753–755.
[26] K. Zheng, D. Zhao, D. Zhang, N. Liu, W. Qin, Journal of Fluorine Chemistry 132 (2011) 5–8.
[27] G. Wang, W. Qin, L. Wang, G. Wei, P. Zhu, R. Kim, Optics Express 16 (2008) 11907–11914.
[28] C. Cao, W. Qin, J. Zhang, Y. Wang, P. Zhu, G. Wang, G. Wei, L. Wang, L. Jin, Journal of Fluorine Chemistry 129 (2008) 204–209.
[29] Y. Wang, L. Tu, J. Zhao, Y. Sun, X. Kong, H. Zhang, Journal of Physical Chemistry C 113 (2009) 7164–7169.
[30] J. Lemyre, A. Ritcey, Chemistry of Materials 17 (2005) 3040–3043.
[31] H. Mai, Y. Zhang, R. Si, Z. Yan, L. Sun, L. You, C. Yan, Journal of the American Chemical Society 128 (2006) 6426–6436.
[32] T. Pang, W. Cao, M. Xing, X. Luo, X. Yang, Optical Materials 33 (2011) 485–489.
[33] C. Zhang, P. Ma, C. Li, G. Li, S. Huang, D. Yang, M. Shang, X. Kang, J. Lin, Journal of Materials Chemistry 21 (2011) 717–723.
[34] W. Di, M. Willinger, R. Ferreira, X. Ren, S. Lu, N. Pinna, Journal of Physical Chemistry C 112 (2008) 18815–18820.
[35] D. Ma, D. Yang, J. Jiang, P. Cai, S. Huang, CrystEngCommunity 12 (2010) 1650–1658.
[36] C. Li, Z. Quan, P. Yang, J. Yang, H. Lian, J. Lin, Journal of Materials Chemistry 18 (2008) 1353–1361.
[37] D. Li, C. Ding, G. Song, S. Lu, Z. Zhang, Y. Shi, H. Shen, Y. Zhang, H. Ouyang, H. Wang, Journal of Physical Chemistry C 114 (2010) 21378–21384.
[38] D. Chen, Y. Wang, Y. Yu, P. Huang, Applied Physics Letters 91 (2007) 051920–051923.